NASA Technical Memorandum 82610

Performance of High Resistivity n+pp+ Silicon Solar Cells Under 1 MeV Electron Irradiation

I. Weinberg, C. Goradia,
C. K. Swartz and A. M. Hermann
Lewis Research Center
Cleveland, Ohio

Prepared for the
Fifteenth Photovoltaic Specialists Conference
sponsored by the Institute of Electrical and Electronics Engineers
Kissimmee, Florida, May 12-15, 1981

NASA

PERFORMANCE OF HIGH RESISTIVITY n^+pp^+ SILICON SOLAR CELLS UNDER 1 MeV ELECTRON IRRADIATION

I. Weinberg, C. Goradia,* C. K. Swartz, and A. M. Hermann**

National Aeronautics and Space Administration
Lewis Research Center
Cleveland, Ohio 44135

ABSTRACT

High resistivity (1250 and 84 ohm-cm) n^+pp^+ silicon solar cells were irradiated by 1 MeV electrons and their performance evaluated as a function of fluence. It was observed that the greatest degradation in power occurred for the higher resistivity cell. The data were analyzed, using a high injection theory, under open-circuit conditions and the components of V_{OC} determined as a function of fluence. It was found that the voltage contributions from the front and back junctions decreased while the base component (V_B) increased with fluence. The anomalous behavior of V_B was attributed to an increase in the base minority carrier gradient ($n_p(o)/n_p(w)$) with fluence. A qualitative argument was presented to support the conclusion that the increased power degradation in the 1250 ohm-cm cells was attributable to an increased voltage drop in the base due principally to an increased lack of conductivity modulation in the cells' base region. Diffusion lengths calculated under high injection conditions were significantly greater than those determined under low injection. This was attributed to a saturation of recombination centers under high injection conditions.

I. INTRODUCTION

Past experience in radiation damage effects indicates that for a given particle energy and fluence cell performance degrades less as cell base resistivity increases. However, previous work on cells with boron-doped base regions has been largely limited to cells with p-base resistivities of 20 ohm-cm or less. Hence, due to the scarcity of information in this area and because of the potential for increase radiation resistance, we have initiated a program aimed at fabrication and analysis of high resistivity cells of varying thicknesses. A major goal of the program was the demonstration that high quality, thin, high resistivity solar cells could be made using processing compatible with conventional practice. To date, 84 and 125.0 ohm-cm n^+pp^+ silicon solar cells have been fabricated with efficiencies between 10 and 12 percent and thicknesses as low as 56 micrometers (1). It is the purpose of the present study to determine the performance and analyze the degradation due to irradiation by 1 MeV electrons for a sampling of cells produced in this program.

II. EXPERIMENTAL PROCEDURES

All cells were fabricated by the Comsat Corp. (1) using spin-on diffusants to form the front n^+ region and back p^+ portion in the boron-doped starting material. The back surface, boron-doped p^+ region was first formed by heating at 900° C for 30 minutes after which the phosphorus diffused n^+ region was formed by heating at 850° C for 15 minutes. Pre-irradiation cell characteristics are listed in table I. Irradiation was performed to a maximum 1 MeV electron fluence of 10^{15} e/cm^2. Solar cell performance parameters were measured before and after each step in the irradiation sequence using a Xenon-arc, AMO solar simulator. Diffusion lengths were measured before and during the irradiation sequence using an X-ray excitation technique (2).

III. EXPERIMENTAL RESULTS

The variation of normalized short circuit currents, I_{SC}, as a function of fluence is shown in figures 1 and 2. Open circuit voltage, V_{OC}, are displayed in figures 3 and 4 while variations in cell maximum power as a function of fluence are plotted in figures 5 and 6. Short circuit current degradation is least for the thinnest cells, especially at the higher resistivity. However, the thickest 1250 ohm-cm cell manifests, by far, the most severe degradation in I_{SC}. Open circuit voltage degradation is greatest, in general, for the 1250 ohm-cm cell irrespective of thickness. Cell maximum powers behave essentially like the voltage, i.e., the lower resistivity cells decidedly exhibit the least degradation.

IV. ANALYSIS AND DISCUSSION

When considering cells with base resistivities well above 10 ohm-cm under AMO light intensities, it is necessary to first ascertain the relative concentration of the injected minority

*Cleveland State University, Cleveland, Ohio 44115 and NASA-ASEE Faculty Fellow.
**Summer Employee, Present Address: Solar Energy Research Institute, Golden, Colorado 80401.

carriers (Δn) and the base majority carriers (p). If Δn is on the order of or greater than p, the base is in high injection and standard low injection theories do not apply. Considering first the present high resistivity cell, Hauser (3) has shown by a computerized, detailed, exact numerical analysis, valid for all injection levels, that the p-base region of a 1000 ohm-cm n^+pp^+ cell is in high injection, at AMO intensities, for cell voltages greater than 0.35 volt. Hence, the present high resistivity cell is in high injection under these conditions. For the present 84 ohm-cm cells, calculations shown in Appendix A of the present paper indicate that the entire base region of these cells is also in high injection for cell voltages greater than approximately 0.5 volts. Since detailed closed-form analytical solutions of the device equations exist, valid under open circuit conditions (4,5), we restrict our calculations to the open circuit case. This procedure enables us to obtain calculated values of diffusion length and to determine specific cell regions where degradation in V_{OC} occurs. We restrict our treatment of degradation in P_{max} to qualitative remarks.

Open Circuit Voltage

Our analysis for cell behavior under open circuit conditions is based on a theory valid for high injection (5). The theory gives closed-form analytical expressions for V_{OC} from which the components of V_{OC} can be calculated. In addition, numerical results obtained from the derived expressions (5) are found to be in agreement with the results of exact numerical solutions of the basic device differential equations (6). Complete expressions in terms of diffusion lengths, diffusivity, carrier concentrations, etc., are given in reference 5. In the following we list only sufficient relations to aid in interpreting the present V_{OC} degradation data.

The device geometry is shown in figure 7, where V_J and V_{JB} are the front and rear junction potentials respectively and V_B is the electrostatic potential drop across the lightly-doped base region. The open circuit voltage is the sum of these potentials, i.e.;

$$V_{OC} = V_J + V_{JB} - V_B \qquad (1)$$

V_B is the Dember potential which appears as a result of inqualities in the electron and hole mobilities. The associated electric field opposes the tendency for electrons to diffuse faster than holes and in this case, is directed away from the front junction. Hence the negative sign accompanying V_B in equation (1).

The components of V_{OC} are given in terms of cell short circuit current, reverse saturation current, carrier and charge densities and mobilities by (5)

$$V_J = \frac{kT}{q} \ln \frac{I_{sc}}{I_o} \qquad (2)$$

$$V_{JB} = \frac{kT}{q} \ln \left(1 + \frac{n_p(w)}{N_{AP}}\right) \qquad (3)$$

$$V_B = \frac{kT}{q}\left(\frac{b-1}{b+1}\right) \ln \left\{ \frac{n_p(o) + \frac{bN_{AP}}{b+1}}{n_p(w) + \frac{bN_{AP}}{b+1}} \right\} \qquad (4)$$

with

$$n_p(w) = \frac{n_p(o)}{\cosh\left(\frac{W}{L_n}\right) + \frac{S_{pp^+}L_n}{D_n} \sinh\left(\frac{W}{L_n}\right)} \qquad (5)$$

Where I_{sc} and I_o are short circuit and dark reverse saturation currents respectively, $n_p(o)$ and $n_p(w)$ are electron densities in the p-base at the front and rear junctions respectively, N_{AP} is the acceptor concentration in the base, $b = \mu_n/\mu_p$ where μ_n and μ_p are electron and hole mobilities, L_n and D_n are diffusion length and diffusivities in the p-region and S_{pp^+} is recombination velocity at the rear surface.

In the preceding equations, V_{OC}, I_{sc}, W and N_{AP} are measured quantities while, μ_n, μ_p and D_n are readily obtainable. S_{pp^+} I_o, $n_p(w)$ and $n_p(o)$ are calculated quantities, expression for which are given in reference 5.

Equations (1) to (5) are expressed in a form which facilitates interpretation of data. The full relation for V_{OC} is a cumbersome lengthy equation which can be seen in reference 5 and will not be repeated here. All terms in the final expression for V_{OC} are either measured or calculated with the exception of L_n which treated as an adjustable parameter in fitting the measured values of V_{OC}. The results for L_n will be discussed in the next section. For the present section, we concern ourselve with the components of V_{OC}. A typical set of calculated values of V_J, V_{JB} and V_B are shown in figures 8 and 9. From equation (2) the front junction contribution, V_J, is higher for the lower resistivity cells primarily because of the lower value of I_o, the dark saturation current, which decreases with decreasing resistivity. On the other hand, from equation (3), V_{JB} is higher for the high resistivity cell due primarily to the lower value of base acceptor concentration in this cell. Although both V_J and V_{JB} tend to decrease with increased fluence, V_B the base component tends to increase with increased fluence. From equation (4), assuming constant mobilities, the variation in V_B arises from a change in base minority carrier concentrations which is reflected by a change in the ratio $n_p(o)/n_p(w)$, the base minority carrier concentration gradient. That this is the case is seen in figure 10 where we have plotted $n_p(o)/n_p(w)$, obtained from equation (5), for the cells of figures 8 and 9. From the figure it is seen that the base minority gradient tends to increase

with fluence. We attribute this principally to the decrease of diffusion length with fluence.

Diffusion Lengths and Damage Coefficients

As mentioned in the previous section, L_n the base minority carrier diffusion length was treated as an adjustable parameter when computing V_{OC}. In the complete expression for V_{OC}, all parameters such as I_{SC}, I_O, $n_p(w)$, $n_p(o)$ are either measurable or computed with the exception of L_n. This latter quantity was varied and the calculation iterated until a value of L_n was found which yielded calculated values of V_{OC} in agreement with the measured values. This procedure yields a set of calculated diffusion lengths under high injection (AMO) conditions. Pre-irradiation values of diffusion length so obtained are listed in table II along with measured low injection values obtained by the X-ray excitation method (2). Using these values and the diffusion length values obtained as a function of fluence, damage coefficients were obtained, for both high and low injection, from the relation

$$\frac{1}{L^2} = \frac{1}{L_o^2} + K_L \phi \qquad (6)$$

where L_o is the pre-irradiation value of diffusion length, L is the diffusion length at fluence ϕ and K_L is the diffusion length damage coefficient. A typical plot of this relation is shown in figure 11 which indicates that the calculated diffusion length values are consistent with equation (6). Damage coefficients for both low and high injection are shown in table II. From the table it is seen that the diffusion lengths obtained under high injection are greater than the low injection diffusion lengths. This is consistent with a filling up or possibly saturation of recombination centers (defect states) under high injection conditions. Under these conditions, one would expect the damage coefficients for high injection to be lower than those obtained under low injection, in agreement with the data in table II. It is also noted that the calculated high injection diffusion lengths appear to be thickness dependent.

Maximum Power

The data presented here for the degradation in P_{max} (figs. 5 and 6) clearly indicates that the degradation, with fluence, is greatest for the 1250 ohm-cm cell, i.e., we observe that degradation increases with resistivity, an effect opposite to that previously observed for low resistivity cells ($\rho < 20$ ohm-cm). The reason for this supposedly anomalous behavior lies in the fact that the voltage drop across the base becomes more significant as the base resistivity increases.

The results of the last section have shown that under open circuit conditions the minority carrier gradient in the base ($n_p(o)/n_p(w)$) increases with fluence and therefore that the minority carrier concentration near the back junction decreases with fluence. It has also been shown that as current flow increases, the region of reduced minority concentration near the back junction tends to increase in size by extending further into the base (7). Under high injection condition, it has further been shown that with increase current, the region of reduced minority, carrier concentration also shows lack of conductivity modulation, leading to an increased voltage drop across the base (7). Hence, at a current flow corresponding to P_{max}, the effect becomes more pronounced leading to a corresponding decrease in P_{max}. This is an effect which occurs principally under high injection conditions with the region of reduced conductivity modulation increasing as base resistivity increases (7). Hence the degradation is greatest for the 1250 ohm-cm cell. Thus it appears that there is a base resistivity value beyond which increases in resistivity do not lead to a reduction in radiation induced P_{max} degradation.

V. CONCLUSIONS

Analysis of data from 84 and 1250 ohm-cm n^+pp^+ cells under open circuit condition has yielded calculated values for the voltage components of V_{OC} and diffusion lengths under high injection conditions. In addition, a qualitative treatment of P_{max} degradation under 1 MeV electron irradiation yielded additional information on the causes of degradation in these cells. From these results it was found that:

Under open-circuit conditions, V_J and V_{JB}, the front and back junction voltages decrease with increased 1 MeV electron fluence, however the base component V_B is found to increase with fluence. Calculations indicate that the increase in V_B can be attributed to an increase in the base minority carrier gradient $n_p(o)/n_p(w)$ with fluence.

Diffusion lengths obtained under high injection conditions are consistently greater than those measured under low injection. Furthermore, the high injection diffusion length damage coefficients are lower than those obtained under low injection. It is speculated that these results could be due to a saturation of recombination centers under high injection conditions.

It was observed that the greatest degradation in P_{max} occurred for the highest resistivity cells. This is opposite to previous observations for cells with $\rho_{Base} < 20$ ohm-cm. A qualitative argument tends to support the conclusion that increased voltage drop in the base due to lack of conductivity modulation in the high resistivity cells is the principal cause of the observed increased degradation.

APPENDIX A - DETERMINATION OF HIGH INJECTION CONDITION IN LIGHTLY DOPED BASE REGION

In general high injection conditions exist when the minority carrier concentration is on the order of, or greater than the majority carrier concentration. Thus to determine when this is so, we calculate the minority carrier concentration n_p, which is obtained from the solution to the equation of continuity;

$$\frac{d^2n_p}{dx^2} - \frac{n_p}{L_n^2} + \frac{\alpha F_o e^{-\alpha x}}{D_n} = 0 \qquad (A1)$$

where L_n and D_n are electron diffusion length and diffusivity, respectively, F_o is the photon flux at wavelength λ and $x = 0$ (see fig. 7) and α the absorption coefficient is also a function of wavelength λ. In writing equation (A1) a quantum efficiency of one is assumed: The solution to equation (A1) is

$$n_p = A_2 \cosh \frac{x}{L_n} + B_2 \sinh \frac{x}{L_n} - k'e^{-\alpha x} \qquad (A2)$$

with

$$k' = \frac{\alpha F_o L_n^2/D_n}{\alpha^2 L_n^2 - 1} \qquad (A3)$$

Using the geometry of figure 7, A_2 and B_2 are found by applying the boundary conditions

$$n_p = n_{po}(e^{qv/kT} - 1); \text{ at } x = 0 \qquad (A4)$$

$$S_B n_p q = -D_n \frac{dn_p}{dx}; \text{ at } x = w \qquad (A5)$$

where n_{po} is the equilibrium electron concentration, v is cell junction voltage and S_B is recombination velocity at the back junction.

The solutions for A_2 and B_2 are

$$A_2 = n_{po}(e^{qv/kT} - 1) + k' \qquad (A6)$$

$$B_2 = -A_2 \frac{\gamma_n}{\delta_n} + \frac{k'}{\delta_n}(S_B - D_n\alpha)e^{-\alpha w} \qquad (A7)$$

with

$$\gamma_n = \frac{D_n}{L_n} \sinh \frac{W}{L_n} + S_B \cosh \frac{W}{L_n} \qquad (A8)$$

$$\delta_n = \frac{D_n}{L_n} \cosh \frac{W}{L_n} + S_B \sinh \frac{W}{L_n} \qquad (A9)$$

In assesing whether or not the cells are in high injection we calculate $n_p(w)$ as a function of voltage, summing F_o over the solar spectrum and α over the range of the cells spectral response. For the 84 ohm-cm cell we use $S_B \approx 0$ with $L_n = 914$ μm from table II. The results are given in the following table.

TABLE AI. - MINORITY CARRIER CONCENTRATIONS IN CELL BASE $\rho_B = 84$ ohm-cm; $N_{AP} = 1.7\times10^{14}/cm^3$; W = 250 μm

V (volts)	$n_p(w)$ cm^{-3}
0.5	2×10^{14}
.45	2.9×10^{13}
.4	1.5×10^{13}

From the table, the entire 84 ohm cm cell is in high injection at voltages equal to or above 0.5 volts.

As a check on these calculations, we repeat them for the 1250 ohm-cm, recalling that Dunbar and Hauser (3) through an exact numerical calculation have shown that at 1000 ohm-cm the entire cell base is in high injection at voltages greater than 0.35 volts.

TABLE AII. - MINORITY CARRIER CONCENTRATION IN CELL BASE $\rho_B = 1250$ ohm-cm; $N_{AP} = 10^{13}/cm^3$; W = 250 μm

V (volts)	$n_p(w)$ cm^{-3}
0.5	3.4×10^{15}
.4	8.2×10^{13}
.3	1.2×10^{13}

The present calculations predict that the cell base is in high injection at voltages equal to or greater then 0.3 volts. This is sufficiently close to the value 0.35 volts found in the more detailed exact calculations (3).

These calculations have been repeated for the remaining cell thicknesses with results similar to that found in this above calculations.

REFERENCES

1. J. F. Allison, R. A. Arndt, and A. Muelenberg, Jr., "Thin n-i-p Radiation Resistant Solar Cell Feasibility Study," NASA CR-159871, 1980.
2. W. Rosenzweig, "Diffusion Length Measurements by Means of Ionizing Radiation," Bell Syst. Tech. J., vol. 41, no. 5, pp. 1573-1588, September 1962.
3. P. M. Dunbar and J. R. Hauser, "A Theoretical Analysis of the Current-Voltage Characteristics of Solar Cells," Annual Report on NASA Lewis Grant NGR 34-002-195, 1975.
4. A. G. Sabnis, "Junction Potentials of Strongly Illuminated n^+-p-p^+ Solar Cells," Solid-State Electron., vol. 21, pp. 581-587, March 1978.
5. C-Y Wu and W-Z She , "The Open Circuit Voltage of Back-Surface-Field (BSF) p-n Junction Solar Cells in Concentrated Sunlight," Solid-State Electron., vol. 23, pp. 209-216, March 1980.
6. J. G. Fossum, E. L. Burgess, and F. A. Lindholm, "Silicon Solar Cell Designs Based on Physical Behavior in Concentrated Sunlight," Solid-State Electron., vol. 21, pp. 729-737, May 1978.

7. R. J. Schwartz, M. S. Lundstrom, and R. D. Nasby, "The Degradation of High Intensity BSF Solar-Cell Fill Factors Due to a Loss of Base Conductivity Modulation, IEEE Trans. Electron Devices, vol. ED-28, no. 3, pp. 264-269, March 1981.

TABLE I. - PRE-IRRADIATION CELL CHARACTERISTICS

ρ, ohm-cm	t, μm	V_{oc}, mV	I_{sc}, mA	FF, percent	EFF, percent	Number of cells
1250	61	577	128.9	74.8	10.3	2
1250	101	579	141.9	72.2	10.8	2
1250	250	580	146.8	69.9	10.9	2
85	56	589	130.5	75.4	10.6	2
85	250	572	152.5	70.2	11.2	3

AR coating: Ta_2O_5.

TABLE II. - DIFFUSION LENGTHS AND DAMAGE COEFFICIENTS

ρ, ohm-cm	t, μm	L(μm)		K_L	
		High injection	Low injection	High injection	Low injection
1250	61	859	224	4×10^{-12}	-------
1250	101	1075	220	5.2×10^{-12}	9×10^{-12}
1250	250	1667	219	5.7×10^{-12}	20×10^{-12}
84	56	610	130	8.4×10^{-12}	18×10^{-12}
84	250	914	155	12×10^{-12}	40×10^{-12}

High injection: from AMO data.
Low injection: from X-ray data.

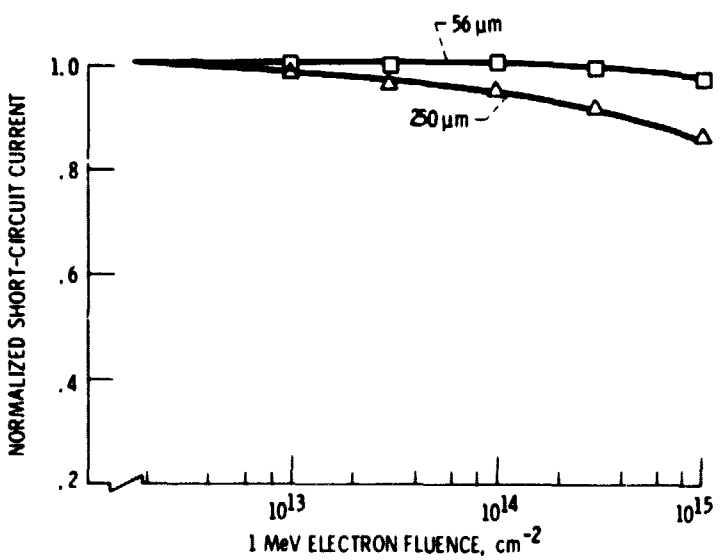

Figure 1. - Variation of short circuit current of 84 Ω-cm n^+pp^+ cells with irradiation.

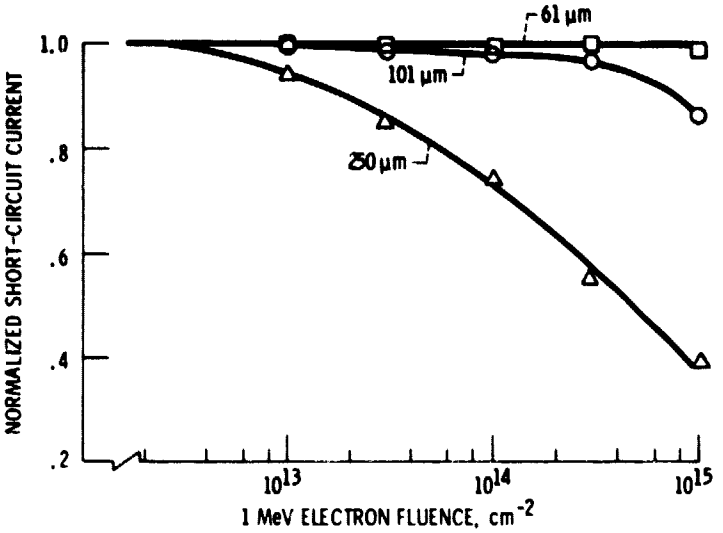

Figure 2. - Variation of short circuit current of 1250 Ω-cm n^+pp^+ cells with irradiation.

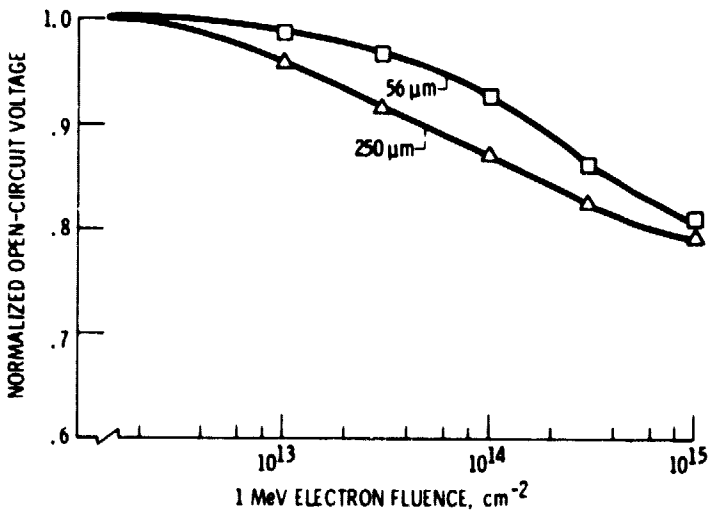

Figure 3. - Variation of open circuit voltage of 84 Ω-cm n^+pp^+ cells with irradiation.

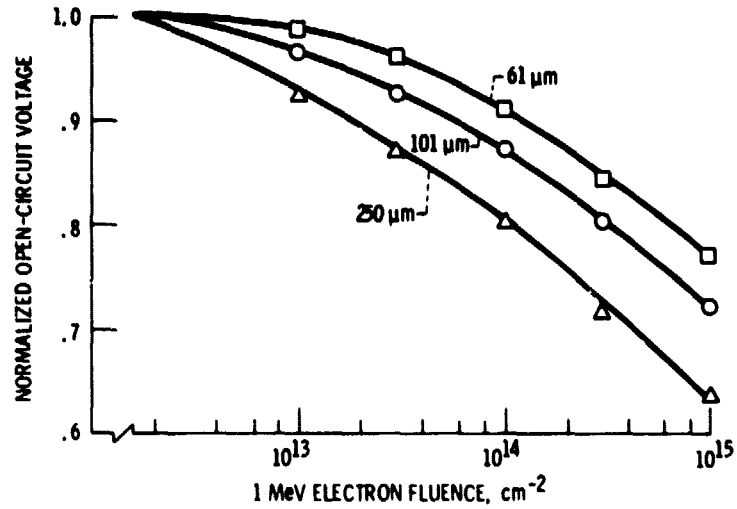

Figure 4. - Variation of open circuit voltage of 1250 Ω-cm n^+pp^+ cells with irradiation.

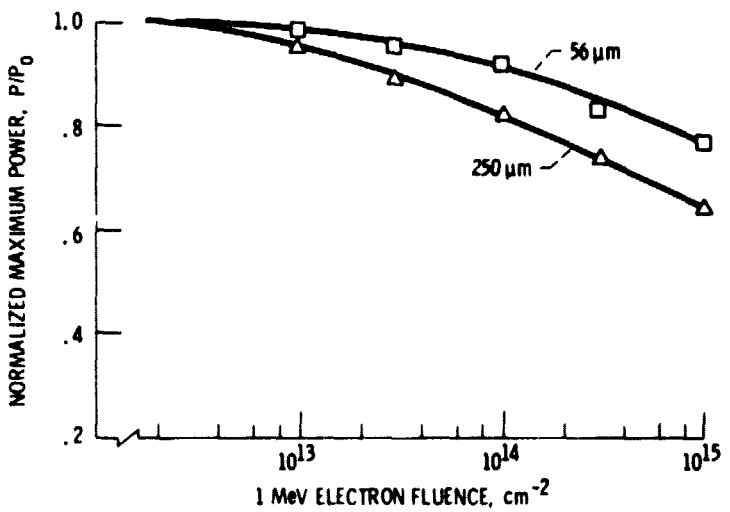

Figure 5. - Variation of maximum power of 84 Ω-cm n^+pp^+ solar cells with irradiation.

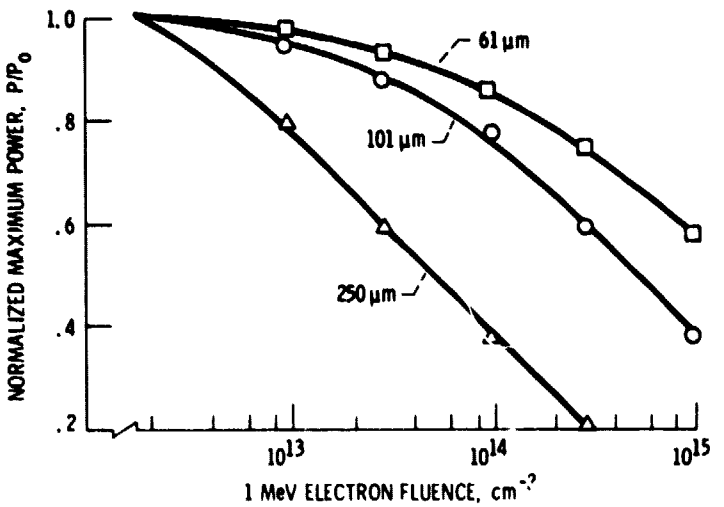

Figure 6. - Variation of maximum power of 1250 Ω-cm n^+pp^+ solar cells with irradiation.

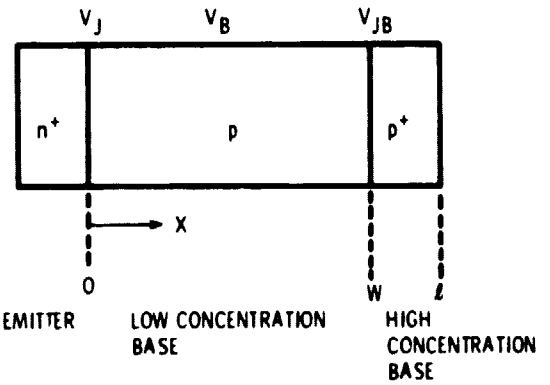

Figure 7. - Device geometry.

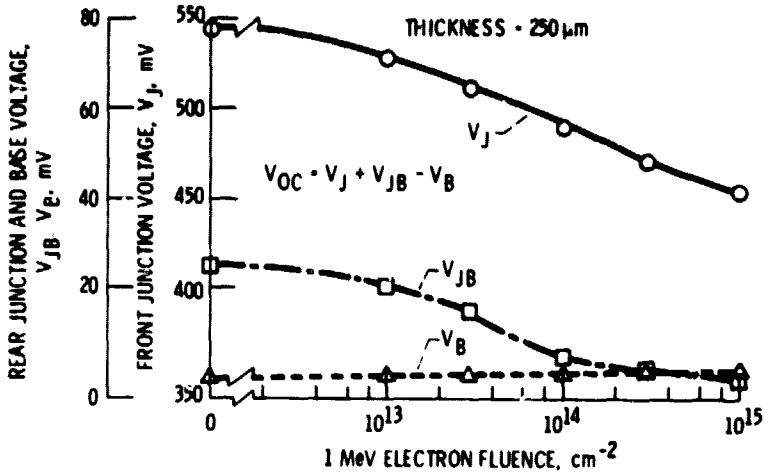

Figure 8. - Components of open-circuit voltage for 84 Ω-cm n^+pp^+ cells.

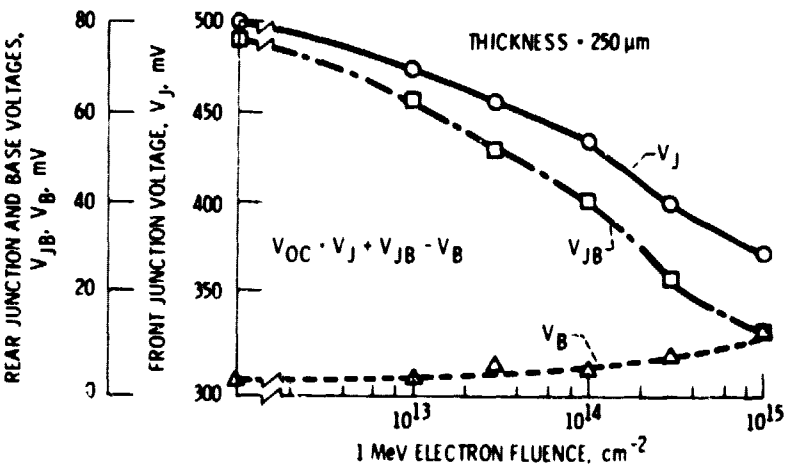

Figure 9. - Components of open-circuit voltage for 1250 Ω-cm n^+pp^+ cells.

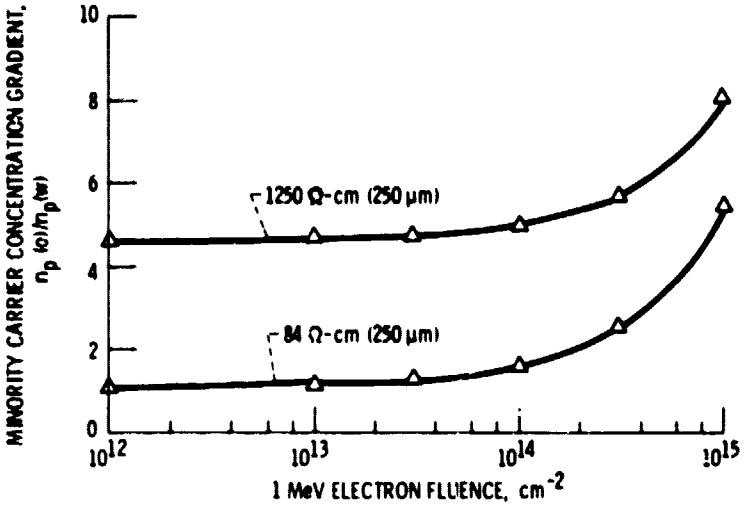

Figure 10. - Fluence dependence of base minority carrier gradient.

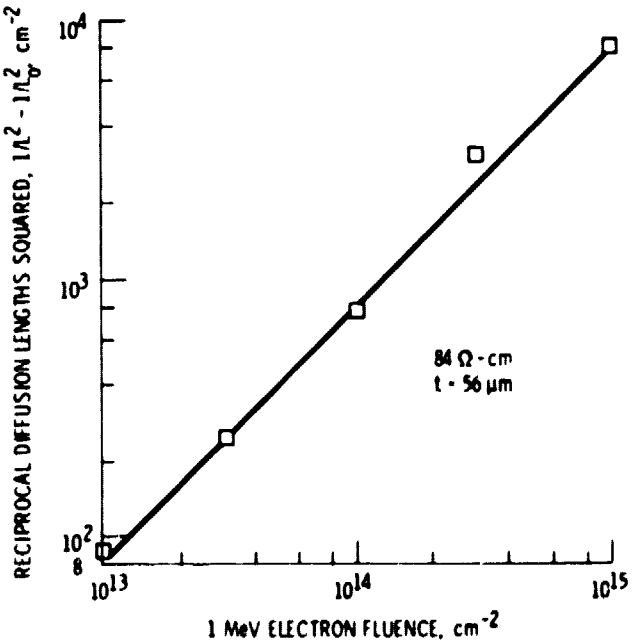

Figure 11. - Variation of calculated diffusion lengths with fluence.